

LETTER TO THE EDITOR

Minimalist model of the W50/SS433 "Extended X-ray Jet": anisotropic wind with recollimation shocks

E. M. Churazov^{1,2}, I. I. Khabibullin^{3,2,1}, and A. M. Bykov⁴

¹ Max Planck Institute for Astrophysics, Karl-Schwarzschild-Str. 1, D-85741 Garching, Germany

² Space Research Institute (IKI), Profsoyuznaya 84/32, Moscow 117997, Russia

³ Universitäts-Sternwarte, Fakultät für Physik, Ludwig-Maximilians-Universität München, Scheinerstr.1, 81679 München, Germany

⁴ Ioffe Institute, Politechnicheskaya st. 26, Saint Petersburg 194021, Russia

January 30, 2024

ABSTRACT

W50 is a radio nebula around hyper-accreting Galactic microquasar SS 433. In this letter, we focus on one peculiar feature of W50 - a pair of so-called "extended X-ray jets" (EXJs). These "jets" have a size of ~ 20 pc, a sharp inner boundary, and their spectra are well represented by a featureless X-ray continuum. We argue that EXJ could be an outcome of a powerful *anisotropic* wind produced by a super-critical accretion disk. The wind itself consists of two components. The first component is a nearly isotropic outflow that subtends most of the solid angle as seen from the compact source. The second component is a more collimated wind aligned with the binary system rotation axis (polar wind). The termination shock of the former component recollimates the latter, giving it an appearance of an extended X-ray structure. In this model, the EXJ continuum spectrum is due to synchrotron emission of electrons accelerated in the recollimated polar wind. At variance with many other studies, in this model, the EXJ structures are not directly related to the highly collimated $0.26c$ baryonic jets. Instead, the EXJ and the W50's ears are produced by the part of the wind with an Eddington level kinetic luminosity confined to a half opening angle of $\sim 10^\circ$, which is not necessarily a recollimated version of the jets.

Key words. ISM: jets and outflows – X-rays: binaries – plasmas – acceleration of particles

1. Introduction

W50 and SS433 represent a prototypical combination of a giant radio-bright nebula and a hyper-accreting compact source that powers the nebula (see, e.g. Margon 1984; Fabrika 2004, for reviews). Many properties of W50/SS433 remain poorly understood though, partly because rare and short-living hyper-accreting black holes or neutron stars might operate in a very different regime than more ubiquitous and better-studied sub-Eddington sources (e.g. Fabrika et al. 2015). In this regard, the stability of SS 433 properties over more than 40 years of observations (e.g. Cherepashchuk et al. 2021) makes it a particularly appealing "laboratory" for hyper-accretor exploration (e.g. Begelman et al. 2006).

It has been shown that the binary system in SS 433 can avoid forming a common envelope and sustain an extremely large accretion rate (\sim few hundred the Eddington level) for a long time, $t_{\text{life}} \sim 10^4$ yrs (van den Heuvel et al. 2017; Cherepashchuk et al. 2023). A simple estimate of the total energy that might be injected by such a source into the surrounding medium, $E_{\text{inj}} \sim L_{\text{Edd}} t_{\text{life}} \sim 3 \times 10^{50} L_{39} t_4$ erg, where $L_{39} = L_{\text{Edd}}/10^{39}$ erg s^{-1} and $t_4 = t_{\text{life}}/10^4$ yr. This is comparable to the energy output of a supernova explosion that has created the compact object of the binary in the first place. As a result, such an object can strongly affect the Interstellar Medium (ISM) in the vicinity of the binary, creating and powering a giant, $\gtrsim 10$ pc, nebula (e.g. Begelman et al. 1980).

A key prediction of the standard accretion theory in the highly super-critical regime (Shakura & Sunyaev 1973) is channeling of

a large fraction of liberated gravitational energy of the accreted material into powerful trans- and mildly relativistic outflows with various degrees of axial collimation (see Yoshioka et al. 2022, for recent numerical simulations). One of the most notable features of SS 433 - the trans-relativistic baryonic jets with bulk velocity $v \sim 0.26c$ and an opening angle of less than 2 degrees - appears to be a direct confirmation of this prediction (e.g. Begelman et al. 1980; Calvani & Nobili 1981). These narrow jets reveal themselves in X-ray and optical spectra as pairs of blue and red-shifted lines, coming from vicinity ($\lesssim 10^{12}$ cm and $\lesssim 10^{15}$ cm for X-ray and optical lines, respectively) of the compact source (Fabrika 2004; Blundell et al. 2018; Waisberg et al. 2019). Modeling of these lines demonstrates that the kinetic luminosity of the jets is indeed comparable to the Eddington luminosity of a stellar-mass black hole (Marshall et al. 2002; Brinkmann et al. 2005; Medvedev & Fabrika 2010; Marshall et al. 2013; Khabibullin et al. 2016; Medvedev et al. 2019; Fogantini et al. 2023). The baryonic jets, however, remain invisible beyond the distance of ~ 0.1 pc from the central source, where they manifest themselves as a spectacular time-variable corkscrew pattern of the radio emission due to the precession of the jets' direction with a period of 163 days and half-amplitude 20 degrees (e.g. Hjellming & Johnston 1981; Blundell & Bowler 2004).¹

¹ The nature of the diffuse X-ray emission detected by the *Chandra* Observatory from a similar location (so-called "arcsec-scale X-ray emission, Migliari et al. 2002) is less clear (e.g. Khabibullin & Sazonov 2017), given its irregular variability and peculiar spectral features (Migliari et al. 2005; Miller-Jones et al. 2008).

Since at even large scales, from 40 to 110 pc, SS 433 is surrounded by the radio- and $H\alpha$ -bright nebula W50 with strong elongation (with 3:1 aspect ratio) along the jets' precession axis, it has been long considered that the kinetic energy of these strongly collimated jets powers/distorts the W50 nebula (Begelman et al. 1980; Zealey et al. 1980; Eichler 1983; Peter & Eichler 1993; Velázquez & Raga 2000; Zavala et al. 2008; Goodall et al. 2011; Asahina et al. 2014; Monceau-Baroux et al. 2015; Panferov 2017; Ohmura et al. 2021).

The question of whether the narrow jets power the entire nebula remains open. Indeed, in the radio, optical and X-ray images of W50, there are no direct observational signatures of the narrow jets' recollimation and/or termination (like termination hot spots or a clear pattern of the decelerating flow, see, e.g., Dubner et al. 1998; Goodall et al. 2011; Farnes et al. 2017; Broderick et al. 2018). Instead, very peculiar elongated X-ray structures are seen on both sides of SS 433 (e.g. Watson et al. 1983; Yamauchi et al. 1994; Safi-Harb & Ögelman 1997; Safi-Harb & Petre 1999; Brinkmann et al. 2007; Safi-Harb et al. 2022). These features, which we further-on call Extended X-ray Jets (EXJ), are separated from the binary by ~ 20 pc, aligned with the narrow jet precession axis, and have an opening angle of $\sim 20^\circ$ (i.e. twice smaller than the precession amplitude of the compact jets). They are characterized by a hard featureless X-ray spectrum that gradually steepens with distance from SS 433 (e.g. Brinkmann et al. 2007; Safi-Harb et al. 2022).

The synchrotron origin of these structures is not only attractive from the spectral and energy/mass requirements points of view (e.g. Brinkmann et al. 2007), but it also leads to verifiable predictions regarding very high energy (VHE) gamma-ray emission coming from them (Safi-Harb & Ögelman 1997; Aharonian & Atoyan 1998; Reynoso et al. 2008; Kimura et al. 2020; Sudoh et al. 2020). Thanks to the advent of modern VHE observatories, the extended lobe-like emission from W50 has been detected at TeV energies (Abeysekara et al. 2018). Another important implication of the synchrotron scenario is the possibility of a high degree of polarization, given that the magnetic field is globally ordered inside these lobes. The recent observation of the eastern lobe by *IXPE* revealed a high degree of X-ray polarization with the direction indicating magnetic field orientation along the main axis of the system (Kaaret et al. 2023).

In this paper, we outline a model that attempts to associate the overall W50 morphology and EXJs with an anisotropic wind from the binary system. In this model, an almost isotropic part of the wind is responsible for the quasi-spherical part of the W50 nebula, while a more collimated portion of the wind drives the "ears" of W50. In the same framework, the termination of the isotropic wind sends recollimation shocks into the collimated wind, giving rise to EXJ features.

2. Basic model

We are trying to explain the following salient characteristics of EXJ associated with W50:

- **Sharp EXJ inner boundary** in X-rays on both sides from SS433 and the lack of bright emission in optical and radio bands.
- **Featureless EXJ X-ray spectrum**, which can (empirically) be described as either thermal bremsstrahlung with $kT \sim 4$ keV or a power law with the photon index $\Gamma \sim 2.2$ (Brinkmann et al. 2007). From the joint analysis of *XMM-Newton* and *NuSTAR* data, Safi-Harb et al. (2022) derived a flatter spectrum $\Gamma \sim 1.6$ for the EXJ portion closest to the

SS433 and $\Gamma \sim 2.05$ for the "lenticular" region that is further away (based on the data of only *XMM-Newton*).

A usual assumption is that an outer boundary of the W50 nebula model is a forward shock associated with the supernova explosion and a jet/outflow (e.g. Goodall et al. 2011). Since the inner boundary of EXJ is closer to the binary than the quasi-spherical part of W50, it is not easy to associate it with any characteristic radius. We assume instead that the entire nebular is powered by a wind produced by SS 433. The wind has an additional characteristic radius - a termination shock, which we want to associate with the inner boundary of EXJ. A wind from a companion star was considered by Konigl (1983), while Asahina et al. (2014) assumed that the wind is produced by the super-Eddington accretion onto the compact object, which is similar to the assumption adopted here. Indeed, for the wind mechanical power of $\sim 10^{39}$ erg s $^{-1}$, the total energy produced by the wind over the estimated age of $\sim 6 \times 10^4$ yr, is $\sim 2 \times 10^{51}$ erg, of the same order or even larger than the kinetic energy of SN ejecta. For the sake of simplicity, we ignore the contribution of the SN energy input, although such a scenario appears more realistic. What matters is that at the present epoch, the powerful wind is present and it has already been operating for a sufficiently long time.

A steady isotropic wind model (Chevalier & Clegg 1985) is characterized by a set of four parameters (assuming that the wind is supersonic): L_w , v_w , t_{age} , and n_0 , which are the wind kinetic power, wind velocity, age of the system, and the density of the interstellar medium (ISM), respectively. The latter is assumed to be homogeneous and uniform. In the frame of this model, one can estimate these four parameters from several basic observables, such as, e.g., the radius of the nebula and the gas temperature downstream of the shock driven by the wind.

A typical radial structure of the wind expanding into a uniform medium is shown in Fig.1. It consists of a forward shock advancing into the ISM, a wind termination shock, and a contact discontinuity, separating the shocked ISM from the shocked wind material. We associate the quasi-spherical part of the W50 nebula with the forward shock. Assuming that we know the downstream temperature of the gas $T_s \sim 0.2$ keV (e.g. Brinkmann et al. 2007; Safi-Harb et al. 2022), the forward shock velocity is

$$v_s = \left(\frac{16}{3} \frac{kT_s}{\mu m_p} \right)^{1/2} \approx 410 \left(\frac{kT_s}{0.2 \text{ keV}} \right)^{1/2} \text{ km s}^{-1}. \quad (1)$$

The estimate of the age of the system for a supersonic expansion, i.e. $R_s \propto t^{3/5}$ is then

$$t_{\text{age}} \approx \frac{3}{5} \frac{R_s}{v_s} = 5 \cdot 10^4 \left(\frac{R_s}{38 \text{ pc}} \right) \left(\frac{v_s}{410 \text{ km s}^{-1}} \right)^{-1} \text{ yr}, \quad (2)$$

while the power of the wind/outflow is

$$L_w \approx \frac{\frac{4}{3} \pi R_s^3 \frac{9}{4} n_0 \mu m_p v_s^2}{t_{\text{age}}} = \quad (3)$$

$$7 \times 10^{38} \left(\frac{n_0}{0.1 \text{ cm}^{-3}} \right) \left(\frac{R_s}{38 \text{ pc}} \right)^2 \left(\frac{kT_s}{0.2 \text{ keV}} \right)^{3/2} \text{ erg s}^{-1}, \quad (4)$$

where n_0 is the particle number density of the unshocked ISM, $\mu \approx 0.61$ is the mean atomic weight per particle. Here we assume that the forward shock is strong and the energy density is constant across the entire volume subtended by the shock. Among the three observables used above, namely R_s , T_s and n_0 , only R_s can be easily measured directly from X-ray or radio images,

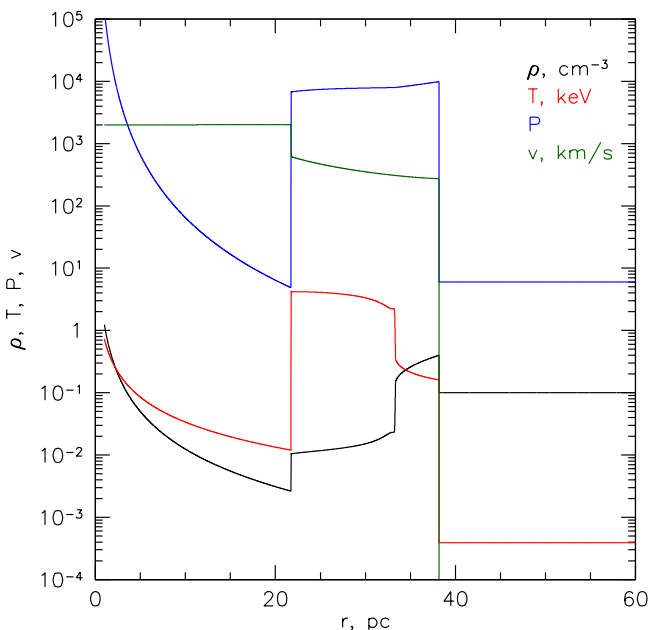


Fig. 1. An example of a spherically symmetric wind model for $n_{\text{ISM}} = 0.1 \text{ cm}^{-3}$, $L_w \sim 10^{39} \text{ erg s}^{-1}$, $v_w = 2 \cdot 10^3 \text{ km s}^{-1}$ after $t_{\text{age}} \sim 6 \cdot 10^4 \text{ yr}$. With these parameters, the densest region is the shell of the shock-compressed ISM on the downstream side of the forward shock, which should dominate the X-ray emission of the nebula. The density of the shocked wind material is too low to produce detectable X-ray emission.

while T_s and n_0 can be robustly determined from X-ray spectra only if the shock-heated ISM has reached collisional ionization equilibrium (and $T_e \approx T_i$), which is not guaranteed a priori. So we use some fiducial values for T_s and n_0 , but acknowledge that their values (except for R_s) are uncertain by a factor of a few. For instance, the density n_0 can be lower, while the post temperature T_s can be higher (see, e.g., a non-equilibrium ionization model in Brinkmann et al. 2007), making the estimate power uncertain in either direction. In particular, their best-fitting estimate of ionization time $n_e t \sim 3 \times 10^{10} \text{ s cm}^{-3}$ for $n_0 = 0.1 \text{ cm}^{-3}$ translates into $t \sim 10^4 \text{ yr}$. It is, therefore, plausible that the actual density of the ambient medium is a factor of a few lower.

The velocity of the wind v_w could be estimated if the radius of the wind termination shock R_T is known. The pressure is approximately constant between the forward shock position R_s and R_T . The latter is determined from the balance of the ram pressure of the wind P_w and the postshock pressure P_s , i.e.

$$P_w = \rho_w v_w^2 = \frac{L_w}{4\pi R_T^2 v_w} \sim P_s = 4 n_0 \frac{3}{16} \mu m_p v_s^2, \quad (5)$$

where $\rho_w(R) \propto R^{-2}$ and v_w are the wind density and velocity, respectively, and the factor of 4 stands for the compression ratio at the forward shock, which is assumed to be strong. The above relation (dropping factors of order unity) implies that the radii of the forward and termination shocks are related via the ratio of the shock and wind velocities as

$$R_T \approx R_s \left(\frac{v_s}{v_w} \right)^{1/2}. \quad (6)$$

The isotropic wind expanding into a homogeneous medium naturally produces a spherically symmetric forward shock, a contact discontinuity, and a termination shock (see Fig. 1). The density of the shocked wind might be low enough so that its thermal

X-ray emission is too faint to be directly observed. Also, the wind isotropic termination shock is not necessarily an efficient particle accelerator (e.g. Parizot et al. 2004). Therefore, in this model, it is not surprising that we see neither radio nor X-ray emissions from this shock.

The W50 nebula is, however, elongated in the direction perpendicular to the orbital plane. This suggests that the wind is anisotropic and, in particular, more powerful (per unit solid angle) along this direction. To explain this morphology, a combination of expanding spherical SN shock and a jet/outflow is often used (e.g. Goodall et al. 2011). Here, we model this configuration as a two-component wind. One component is a nearly isotropic wind considered above (hereafter "i-wind"), while the second component is a collimated polar wind (hereafter "p-wind") along the orbital momentum of the binary. The main difference from the other models is the presence of a termination shock of the isotropic wind that recollimates the p-wind. We reiterate here, that the postulated "p-wind" is not the highly collimated subrelativistic jet, but a part of the wind associated with inner regions of the accretion flow that subtends a much larger solid angle than the narrow jets.

We assume that the termination radius for the p-wind is larger than for the nearly isotropic component (i.e., the dynamic pressure ρv^2 at a given radius is larger for the p-wind). This means that the material in the collimated component will "see" a sudden increase of the ambient pressure when crossing the termination shock of the i-wind. In aerodynamics, this corresponds to the case of an "over-expanded jet", when the internal jet pressure at the edge of the nozzle is lower than the ambient pressure. This large pressure will send a recollimation shock into the p-wind, compressing and heating it. Therefore, an additional characteristic radius appears in the problem, which we associate with the inner boundary of EXJs well inside the forward shock. This is the essence of the proposed model.

In lieu of a sketch, we run a 2D simulation (cylindrical symmetry) using the PLUTO code (Mignone et al. 2007). The density distribution corresponding to $t_{\text{age}} \sim 6 \times 10^4 \text{ yr}$ is shown in Fig. 2. The parameters of the isotropic i-wind are as follows: the kinetic luminosity $10^{39} \text{ erg s}^{-1}$ and the wind velocity $2 \times 10^3 \text{ km s}^{-1}$. The collimated p-wind component is confined to a cone with a half-opening angle of $\sim 10^\circ$. There are various ways of shifting the termination shock of the p-wind to larger radii than the i-wind termination shock. In our illustrative simulation, the density and velocity of the p-wind are both a factor of 3 higher than that in the i-wind. We note here that the model is flexible enough to reproduce the overall morphology of the nebular for different sets of parameters, e.g. a faster p-wind with a half-opening angle of $\sim 6^\circ$ or a much denser and slower p-wind. However, all these models share several common features that are clearly illustrated by Fig. 2. In this figure, the termination shock of the isotropic wind corresponds to the transition from the lowest density region (isotropic wind component just before the shock) to the 4 times larger density (downstream from the termination shock). The collimated outflow goes through a series of recollimation shocks and Mach disks, where the dense regions are interleaved with the lower-density patches. While the first dense region R_d does not occur exactly at the position of the isotropic wind termination shock, they are related, so that $R_d \sim O(1) \times R_T$, where the pre-factor sensitively depends on the p-wind opening angle. The choice of the parameters for this simulation is rather arbitrary and other combinations can lead to a similar morphology when the density or velocity ratios between the i-wind and p-wind are changed together with the characteristic opening angle of the p-wind. However, the recollimation shocks are always present

when the i-wind termination shock is located at a smaller radius than that of the p-wind. Furthermore, this model completely neglects the contribution of the supernova explosion to W50. Adding $\sim 10^{51}$ erg in the form of the SN ejecta can certainly contribute to nebular size and shape, but if the wind is established a sufficiently long time ago (but after the SN explosion), the overall morphology may remain similar to the one depicted in Fig. 2.

3. Discussion

Several models have been proposed to explain the spectrum of EXJ (e.g. Safi-Harb et al. 2022, and references therein), which attribute it to synchrotron emission, however, the origin of the EXJ itself, which "appears in the middle of nowhere" is not easily explained.

Previously, we have considered an exotic scenario for the formation of EXJ, when a very fast (sub-relativistic) outflow recombines and impacts the ISM in the form of a beam of neutral atoms (Churazov et al. 2020). In that model, *neutral* particles penetrate the ISM, get ionized, and deposit their energy in a long and narrow "channel" along the direction of the beam. The heated ISM expands sideways, reducing the gas density and letting neutral particles propagate further without being ionized. This (i) leads to a fast propagation of the heating front and (ii) gives rise to a system of diverging and converging shocks perpendicular to the beam. This analysis was not specifically tied to W50/SS433, except for the assumption that neutral particles are moving with the velocity $\sim 0.25 c$. In the neutral beam model, the EXJ structure forms where the beam enters the dense medium. Therefore, to explain the inner boundary of the EXJ one has to postulate the presence of dense gas at this location.

The model, discussed in the previous section is different. It does not rely on the SS433 trans-relativistic baryonic jets. Instead, it associates EXJ with the recollimation shocks in the anisotropic wind coming from the SS433 binary system. In this model, the isotropic part of the wind reaches the termination shock earlier than the polar wind. This translates into a condition that momentum flux per unit solid angle is larger for the p-wind

$$\rho_p v_p^2 > \rho_i v_i^2, \quad (7)$$

which is equivalent to the condition

$$\frac{L_p}{\Omega_p v_p} > \frac{L_i}{\Omega_i v_i}. \quad (8)$$

In the illustrative example shown in Fig. 2 $\rho_p v_p \approx 30 \rho_i v_i$, so the above condition is satisfied.

Downstream of the termination shock in the isotropic wind, the gas becomes hot and 4 times denser. As mentioned above, the gas density is too low to give rise to observable thermal (bremsstrahlung) emission. The termination shock of the i-wind resembles the case of an almost perpendicular shock (upstream magnetic field is along the shock front) similar to stellar winds around massive stars. No signature of synchrotron X-ray emission was ever reported from the termination shocks of fast radiative-driven winds of young massive stars. Particle acceleration there is likely much less efficient than that in supernova shocks of similar velocity (e.g. Drury et al. 2001; Parizot et al. 2004). Cosmic ray acceleration in the vicinity of the solar wind termination shock (of speed above 400 km s^{-1}) directly measured by the Voyagers is also rather modest (Rankin et al. 2022). Thus the i-wind termination shock can have a low efficiency of particle acceleration. On the contrary, the system of recollimation shocks formed

due to i- and p-winds collision can have a much more complicated structure of magnetic fields, involving both quasi-parallel and quasi-perpendicular region. Here, we simply assume that the acceleration of particles in the recollimated p-wind proceeds similarly to quasi-parallel shocks with a compression factor of 4 (might be larger if CR escape effects are accounted for) and the characteristic shock velocity v_p .

The gas in the p-wind experiences oblique recollimation shocks and Mach disks driven by the isotropic wind, it heats up and goes through a sequence of compression and rarefactions. Similarly to the i-wind, the shocked p-wind density is far too low to produce appreciable thermal emission. We, therefore, rely on the possibility that recollimation shocks are effective in accelerating particles and the EXJ emission is non-thermal (as suggested before, see e.g. Safi-Harb et al. 2022, and references therein). Indeed, recent detection of X-ray polarization from EXJ Kaaret et al. (2023) with *IXPE*, shows that X-ray emission has a synchrotron origin, while the magnetic field is largely along the Eastern EXJ. The acceleration could be due to shocks (i.e. Diffusive Shock Acceleration or DSA Krymskii 1977; Bell 1978) or due to a shear flow (Berezhko 1981; Stawarz & Ostrowski 2002; Rieger & Duffy 2019) that naturally appears in the configuration considered here. In both cases, it is plausible that the acceleration is not confined only to a localized region at the first recollimation shock but is distributed along the EXJ.

The hard non-thermal X-ray emission up to 30 keV from a "knotty" region within the Eastern EXJ was detected with the *NuSTAR* telescope and attributed to synchrotron radiation of very high energy electrons with Lorentz factors above 10^7 (Safi-Harb et al. 2022; Sudoh et al. 2020). These electrons have to be (re)accelerated locally. An ensemble of the recollimation shocks that have to be present after the collision of the p-wind with the termination shock of the i-wind is a plausible site of particle acceleration and magnetic field amplification. Non-thermal X-ray emission observed as thin filaments at the edge of the shell-type young supernova remnants is almost certainly produced by synchrotron emission of TeV regime electrons radiating in highly amplified magnetic field (Reynolds 2008; Helder et al. 2012; Ferrazzoli et al. 2023). Particle acceleration by strong shocks of velocity well above a few thousand km s^{-1} in young supernova remnants is likely accompanied by strong amplification of magnetic fluctuations resulting in Bohm-like diffusion of accelerated particles in a wide interval of particle energies (see e.g. Bykov et al. 2014; Caprioli & Spitkovsky 2014). In the case of Bohm diffusion, the acceleration time t_a of a particle with Lorentz factor γ by a shock of velocity v_p scales with the magnetic field strength B as $t_a \propto \gamma v_p^{-2} \eta B^{-1}$. Here the diffusion coefficient of a relativistic particle of mass m is $D = \eta c^2 m \gamma / e B$, where the dimensionless factor $\eta \geq 1$. The maximal Lorentz factor achievable by the electrons and positrons accelerated by the shock is limited by the synchrotron losses is $\gamma_m \propto v_p B^{-1/2} \eta^{-1/2}$. Therefore, in a single zone model (where particle acceleration and the synchrotron radiation are spatially coincident) the maximal energy of the synchrotron photon E_m depends mostly on the shock velocity $E_m \propto v_p^2 / \eta$. To get $E_m \approx 30 \text{ keV}$ one needs $v_p \sim 20,000 \eta^{1/2} \text{ km s}^{-1}$. The energy flux of the amplified magnetic field in the shock downstream may reach 0.1 of the shock ram pressure (Bykov et al. 2014), which is consistent with observations of young supernova remnants (Helder et al. 2012). In this case, the magnetic field just in the downstream of the recollimation shock can be estimated from the relation $B^2 / 8\pi \approx 0.4 \frac{L_p}{\Omega_i R_i^2 v_p}$. The magnitudes of the fluctuating magnetic field amplified by cosmic-ray-driven

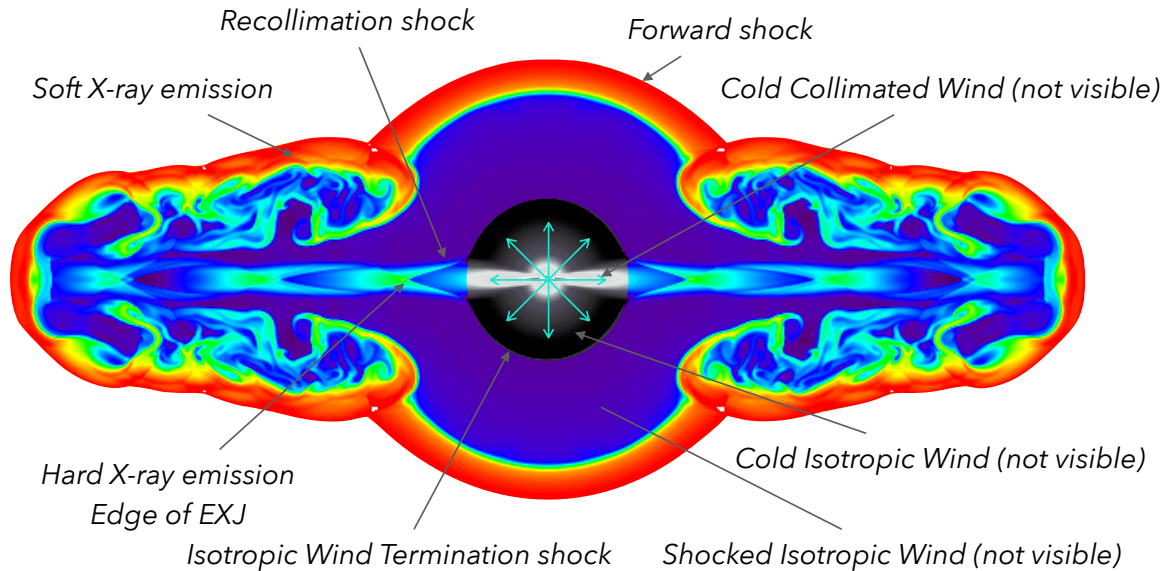


Fig. 2. Sketch of the W50 model as a combination of isotropic and polar winds. The central (black and white) region represents a combination of an isotropic wind and a more collimated "polar" wind aligned with the binary system orbital axis. The isotropic wind passes through its termination shock and increased pressure recollimates the polar wind. Resulting recollimation shocks accelerate particles and give rise to the synchrotron emission of the EXJs.

instabilities may reach $\sim 100 \mu\text{G}$. Then the accelerated electrons radiating 30 keV synchrotron photons should have energies $\sim 100 \text{ TeV}$. The spectra of electrons accelerated by the DSA Fermi mechanism are consistent with those derived from hard X-ray observations (Safi-Harb et al. 2022; Kayama et al. 2022).

The protons accelerated above 100 TeV in the recollimation region will leave the accelerator and can contribute to multi-TeV regime emission detected by HAWC (Abeysekara et al. 2018) and LHAASO (Cao et al. 2023). Assuming the lifetime of EXJ $\sim 10^4 - 10^5 \text{ yr}$, these protons will radiate about $10^{-4} \times n$ of their power due to inelastic hadronic collisions in $\sim 30 \text{ pc}$ vicinity of the knot filled with a plasma of number density n (measured in cm^{-3}) provided that the diffusion coefficient of the high energy protons is $D \sim 10^{27} \text{ cm}^2 \text{ s}^{-1}$ or smaller. The value is generally consistent with that estimated in the vicinity of typical TeV-halos (see e.g. Abeysekara et al. 2017; Martin et al. 2022). We note here that the studied TeV-halos are produced by the rotation power of pulsars and have much lower kinetic/magnetic power than that of W50/SS433 which is powered by hyper-accretion. In this model, the power of the accelerated very high energy nuclei which can reach $\sim 10^{37} \text{ erg s}^{-1}$. Eventually, these nuclei can leave W50/SS433 and contribute to the galactic cosmic ray population.

To make the simplified quantitative estimations of particle acceleration and high energy radiation given above we limit ourselves to the DSA model description. Nonlinear DSA models constructed for single plane shocks account for cosmic ray driven instabilities (see e.g. Schure et al. 2012) that may highly amplify ambient magnetic field fluctuations and thus govern the high energy particle transport. The recollimation of p-wind is accompanied by the formation of a system of oblique shocks and the description of particle acceleration in the wind recollimation region is more complex than the DSA model used above. Namely, the spectra formation at the highest energy end can be affected by CR interaction with the shear flows (see e.g. Rieger & Duffy 2019) which is associated with the p-wind recollimation region.

Accurate modeling of particle spectra would require both high-resolution simulations of the recollimation region for different possible magnetization of p-wind and kinetic modeling of high-energy particle transport in the region.

4. Conclusions

We outline a possible model of Extended X-ray Jets (EXJs) in the W50 Nebula. At variance with other popular models, we do not associate these structures with the well-collimated $0.26 c$ baryonic jets produced by the hyperaccreting binary SS433. It is proposed instead that a powerful anisotropic wind from the binary that was active for a few tens of kyrs is responsible for these structures (and overall W50 morphology as well). In the simplest version of this model, the wind consists of two components: an almost isotropic wind that subtends most of the solid angle and a more collimated "polar" wind. Both wind components are cold and "invisible" until the isotropic wind reaches its terminal shock. Beyond this point, conical recollimation shock is launched into the polar wind component, which is capable of accelerating relativistic electrons powering spectrally featureless and polarized synchrotron radiation visible in X-rays as EXJs.

The inner edges of the EXJs correspond approximately to the location of the first recollimation shock "knot". Plausibly, as suggested earlier, the TeV emission is produced by the same electrons due to IC scatterings of CMB photons. This model also associates the overall shape of the W50 Nebula (a sphere plus two "ears") with the same anisotropic wind, namely the forward shock of the wind propagating into the undisturbed ISM. A particular set of parameters used here for illustration is loosely constrained and likely does not match exactly those in W50. However, we believe that recollimation of the anisotropic wind offers an attractive explanation of the peculiar properties of the Extended X-ray jets in SS433/W50. It is plausible that other hyperaccreting systems can give rise to similar structures as long as the wind has a sufficiently strong angular modulation pattern. The model also stipulates that W50 EXJs are powerful sources of very high-energy cosmic ray protons, which are accelerated within the same converging flow region.

Acknowledgements

I. K. acknowledges support by the COMPLEX project from the European Research Council (ERC) under the European Union's Horizon 2020 research and innovation program grant agreement ERC-2019-AdG 882679. A. B. was supported by the baseline project FFUG-2024-0002 at Ioffe Institute. Some modeling was made at the Supercomputing Center of the Peter the Great Saint-Petersburg Polytechnic University.

References

- Abeyssekara, A. U., Albert, A., Alfaro, R., et al. 2017, *Science*, 358, 911
- Abeyssekara, A. U., Albert, A., Alfaro, R., et al. 2018, *Nature*, 562, 82
- Aharonian, F. A. & Atayan, A. M. 1998, *New A Rev.*, 42, 579
- Asahina, Y., Ogawa, T., Kawashima, T., et al. 2014, *ApJ*, 789, 79
- Begelman, M. C., King, A. R., & Pringle, J. E. 2006, *MNRAS*, 370, 399
- Begelman, M. C., Sarazin, C. L., Hatchett, S. P., McKee, C. F., & Arons, J. 1980, *ApJ*, 238, 722
- Bell, A. R. 1978, *MNRAS*, 182, 147
- Berezhko, E. G. 1981, in *International Cosmic Ray Conference*, Vol. 3, *International Cosmic Ray Conference*, 506
- Blundell, K. M. & Bowler, M. G. 2004, *ApJ*, 616, L159
- Blundell, K. M., Laing, R., Lee, S., & Richards, A. 2018, *ApJ*, 867, L25
- Brinkmann, W., Kotani, T., & Kawai, N. 2005, *A&A*, 431, 575
- Brinkmann, W., Pratt, G. W., Rohr, S., Kawai, N., & Burwitz, V. 2007, *A&A*, 463, 611
- Broderick, J. W., Fender, R. P., Miller-Jones, J. C. A., et al. 2018, *MNRAS*, 475, 5360
- Bykov, A. M., Ellison, D. C., Osipov, S. M., & Vladimirov, A. E. 2014, *ApJ*, 789, 137
- Calvani, M. & Nobili, L. 1981, *Ap&SS*, 79, 387
- Cao, Z., Aharonian, F., An, Q., et al. 2023, *arXiv e-prints*, arXiv:2305.17030
- Caprioli, D. & Spitkovsky, A. 2014, *ApJ*, 794, 47
- Cherepashchuk, A., Belinski, A., Dodin, A., & Postnov, K. 2023, *New A*, 103, 102060
- Cherepashchuk, A. M., Belinski, A. A., Dodin, A. V., & Postnov, K. A. 2021, *MNRAS*, 507, L19
- Chevalier, R. A. & Clegg, A. W. 1985, *Nature*, 317, 44
- Churazov, E., Khabibullin, I., & Sunyaev, R. 2020, *MNRAS*, 495, L51
- Drury, L. O., Ellison, D. E., Aharonian, F. A., et al. 2001, *Space Sci. Rev.*, 99, 329
- Dubner, G. M., Holdaway, M., Goss, W. M., & Mirabel, I. F. 1998, *AJ*, 116, 1842
- Eichler, D. 1983, *ApJ*, 272, 48
- Fabrika, S. 2004, *Astrophys. Space Phys. Res.*, 12, 1
- Fabrika, S., Ueda, Y., Vinokurov, A., Sholukhova, O., & Shidatsu, M. 2015, *Nature Physics*, 11, 551
- Farnes, J. S., Gaensler, B. M., Purcell, C., et al. 2017, *MNRAS*, 467, 4777
- Ferrazzoli, R., Slane, P., Prokhorov, D., et al. 2023, *ApJ*, 945, 52
- Fogantini, F. A., García, F., Combi, J. A., et al. 2023, *A&A*, 669, A149
- Goodall, P. T., Alouani-Bibi, F., & Blundell, K. M. 2011, *MNRAS*, 414, 2838
- Helder, E. A., Vink, J., Bykov, A. M., et al. 2012, *Space Sci. Rev.*, 173, 369
- Hjellming, R. M. & Johnston, K. J. 1981, *ApJ*, 246, L141
- Kaaret, P., Ferrazzoli, R., Silvestri, S., et al. 2023, *arXiv e-prints*, arXiv:2311.16313
- Kayama, K., Tanaka, T., Uchida, H., et al. 2022, *PASJ*, 74, 1143
- Khabibullin, I., Medvedev, P., & Sazonov, S. 2016, *MNRAS*, 455, 1414
- Khabibullin, I. I. & Sazonov, S. Y. 2017, *Astronomy Letters*, 43, 388
- Kimura, S. S., Murase, K., & Mészáros, P. 2020, *ApJ*, 904, 188
- Konigl, A. 1983, *MNRAS*, 205, 471
- Krymskii, G. F. 1977, *Akademiia Nauk SSSR Doklady*, 234, 1306
- Margon, B. 1984, *ARA&A*, 22, 507
- Marshall, H. L., Canizares, C. R., Hillwig, T., et al. 2013, *ApJ*, 775, 75
- Marshall, H. L., Canizares, C. R., & Schulz, N. S. 2002, *ApJ*, 564, 941
- Martin, P., Tibaldo, L., Marcowith, A., & Abdollahi, S. 2022, *A&A*, 666, A7
- Medvedev, A. & Fabrika, S. 2010, *MNRAS*, 402, 479
- Medvedev, P. S., Khabibullin, I. I., & Sazonov, S. Y. 2019, *Astronomy Letters*, 45, 299
- Migliari, S., Fender, R., & Méndez, M. 2002, *Science*, 297, 1673
- Migliari, S., Fender, R. P., Blundell, K. M., Méndez, M., & van der Klis, M. 2005, *MNRAS*, 358, 860
- Mignone, A., Bodo, G., Massaglia, S., et al. 2007, *ApJS*, 170, 228
- Miller-Jones, J. C. A., Migliari, S., Fender, R. P., et al. 2008, *ApJ*, 682, 1141
- Monceau-Baroux, R., Porth, O., Meliani, Z., & Keppens, R. 2015, *A&A*, 574, A143
- Ohmura, T., Ono, K., Sakemi, H., et al. 2021, *ApJ*, 910, 149
- Panferov, A. A. 2017, *A&A*, 599, A77
- Parizot, E., Marcowith, A., van der Swaluw, E., Bykov, A. M., & Tatischeff, V. 2004, *A&A*, 424, 747
- Peter, W. & Eichler, D. 1993, *ApJ*, 417, 170
- Rankin, J. S., Bindi, V., Bykov, A. M., et al. 2022, *Space Sci. Rev.*, 218, 42
- Reynolds, S. P. 2008, *ARA&A*, 46, 89
- Reynoso, M. M., Romero, G. E., & Christiansen, H. R. 2008, *MNRAS*, 387, 1745
- Rieger, F. M. & Duffy, P. 2019, *ApJ*, 886, L26
- Safi-Harb, S., Mac Intyre, B., Zhang, S., et al. 2022, *ApJ*, 935, 163
- Safi-Harb, S. & Ögelman, H. 1997, *ApJ*, 483, 868
- Safi-Harb, S. & Petre, R. 1999, *ApJ*, 512, 784
- Schure, K. M., Bell, A. R., O' C Drury, L., & Bykov, A. M. 2012, *Space Sci. Rev.*, 173, 491
- Shakura, N. I. & Sunyaev, R. A. 1973, *A&A*, 24, 337
- Stawarz, L. & Ostrowski, M. 2002, *ApJ*, 578, 763
- Sudoh, T., Inoue, Y., & Khangulyan, D. 2020, *ApJ*, 889, 146
- van den Heuvel, E. P. J., Portegies Zwart, S. F., & de Mink, S. E. 2017, *MNRAS*, 471, 4256
- Velázquez, P. F. & Raga, A. C. 2000, *A&A*, 362, 780
- Waisberg, I., Dexter, J., Olivier-Petrucci, P., Dubus, G., & Perraut, K. 2019, *A&A*, 624, A127
- Watson, M. G., Willingale, R., Grindlay, J. E., & Seward, F. D. 1983, *ApJ*, 273, 688
- Yamauchi, S., Kawai, N., & Aoki, T. 1994, *PASJ*, 46, L109
- Yoshioka, S., Mineshige, S., Ohsuga, K., Kawashima, T., & Kitaki, T. 2022, *PASJ*, 74, 1378
- Zavala, J., Velázquez, P. F., Cerqueira, A. H., & Dubner, G. M. 2008, *MNRAS*, 387, 839
- Zealey, W. J., Dopita, M. A., & Malin, D. F. 1980, *MNRAS*, 192, 731